AIAA JOURNAL
Vol. 38, No. 10, October 2000

# Postbuckling Strength of Stiffened Composite Plates with Impact Damage

Cheol-Won Kong,* Chang-Sun Hong,† and Chun-Gon Kim‡
*Korea Advanced Institute of Science and Technology, Taejon 305-701, Republic of Korea*

**The buckling and postbuckling strengths for unstiffened and stiffened composite plates with various impact damages were studied numerically and experimentally. To predict the residual strength, a progressive failure model with the degradation of elastic moduli in the damaged regions was adopted in a nonlinear finite element method. The progressive failure analysis used the maximum stress criterion and the complete unloading model. The degradation ratio in each sublaminate was determined by delamination distributions through the thickness of laminates. The ply-by-ply delamination was detected by an improved ultrasonic technique. The predicted buckling and postbuckling strength showed good agreement with experimental results. The correlation between the impact damage and the postbuckling strength is discussed. The delamination growth was also observed for I-stiffened composite plates under the cyclic compressive load.**

## Introduction

THE damage tolerance of composite aircraft structures is addressed by requiring ultimate strength capability in the presence of barely visible impact damage (BVID).[1] Impact damage is one of the major factors degrading the compressive strength of composite structures. The compression after impact (CAI) strength of composite plates has been studied by experimentation and analysis.[2–5] However, a limited number of papers have reported on the prediction of CAI strength based on nondestructive evaluation (NDE) data and the effect of impact damage on the stiffened composite plates. Pavier and Clarke[6] predicted the postimpact compressive strength by using the finite element method. Impact damage was modeled based on the deply technique. The experiment showed that the predictions of the delamination growth did not always allow the prediction of the final failure. Xiong et al.[7] modeled the impact damage by an elliptical soft inclusion. A sublaminate buckling analysis determined the degradation ratio of the elastic moduli in the inclusion. To predict the compressive strength of composite plates damaged by impact, De Moura et al.[8] used interface elements compatible with three-dimensional solid elements for delamination modeling in the finite element analysis. A progressive failure was analyzed on the basis of the triaxial stress state. Experiments were performed on carbon/epoxy laminates with one delamination. To predict the residual strength of thick composite plates, Gottesman et al.[9] used an analytical model based on the information obtained from NDE. Scarponi et al.[10] evaluated the impact damage by using double side inspections and two mode inspections in C-SCAN.

It was difficult to predict the impact characteristics or the CAI strength of stiffened plates from the data of unstiffened plates. Madan and Shuart[11] showed that the skin bay impact produced great strength reductions and that no damage growth occurred before ultimate failure. Greenhalgh et al.[12,13] recommended that the impact damages of unstiffened plates did not represent stiffened plates. The effects of impact locations on the compressive strength of stiffened composite plates were studied by experiments. Ishikawa et al.[14] conducted the CAI experiments on stiffened panels that were made of carbon/epoxy and carbon/peek. Initial buckling stress was predicted by the finite element analysis. Found et al.[15] performed impact tests on the carbon fiber reinforced plastics (CFRP) stiffened panels and the unstiffened panels. Starnes et al.[16] found that low-velocity impact damage reduced the postbuckling strength of a stiffened plate.

In the present study, the degradation model of the elastic moduli in the impact-damaged region was adopted in a nonlinear finite element analysis. The degradation ratio was determined by delamination distributions through the thickness. Delamination distributions through the thickness were detected by an improved ultrasonic inspection. Nonlinear finite element formulation was based on the updated Lagrangian description and the modified arc-length method. A progressive failure analysis was introduced into the nonlinear finite element analysis. This model was applied to unstiffened and stiffened plates with various levels of impact energies. The buckling and postbuckling residual strengths of blade-stiffened composite plates are discussed. The delamination shapes and growths of I-stiffened composite plates under cyclic compression were also observed according to impact locations.

## Finite Element Analysis

The delamination growth or the typical failure analysis with postbuckling analysis can predict the postbuckling compresive strength with impact damage. Recently, some researchers[17–21] analyzed single or multiple delaminations. Although delamination growth is one of the main factors controlling the final failure, the prediction of the delamination growth does not always determine the final failure of the impact-damaged laminates. Many experiments showed that only limited delamination growth occurred before the final failure. In this case, the impact-damaged region could be simply modeled by stiffness reduction, but it was difficult to determine the degree of stiffness reduction in the damaged region. Therefore, the impact-damaged region was assumed as a cutout, or the degree of the stiffness reduction was determined by using compression test data.

In the present analysis, the ratio of the stiffness reduction was determined by using delamination distributions through the thickness as shown in Fig. 1. Each delamination size through the thickness was obtained from C-SCAN. To determine the modulus retention ratio in each sublaminate, nearby delamination sizes were used. It was assumed that the delaminated plies, which may contain matrix cracking, did not carry the compressive load. The modulus degradation region was regarded as the two-dimensional projected delamination area obtained from C-SCAN. Therefore, the modulus retention ratio in each sublaminate is expressed as

$$R_i = 1 - (A_i + A_{i-1})/(2A_{\text{ref}})$$

$$A_0 = A_1, \qquad A_n = A_{n-1}, \qquad i = 1, 2, \ldots, n \tag{1}$$

where $A_{\text{ref}}$ is the two-dimensional projected delamination area, $A_i$ is the area of the $i$th delamination, and $R_i$ is the modulus retention

Received 2 July 1999; revision received 13 January 2000; accepted for publication 5 February 2000. 

*Research Assistant, Department of Aerospace Engineering, 373-1 Kusong-dong, Yusong-gu.
†Professor, Department of Aerospace Engineering, 373-1 Kusong-dong, Yusong-gu. Senior Member AIAA.
‡Associate Professor, Department of Aerospace Engineering, 373-1 Kusong-dong, Yusong-gu. Senior Member AIAA.

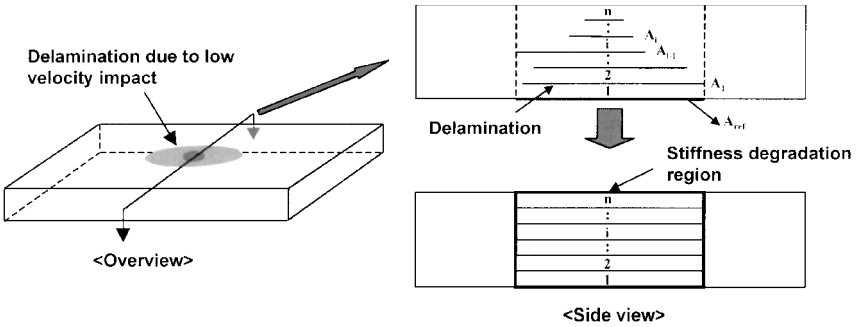


**Fig. 1 Stiffness reduction model in finite element analysis.**

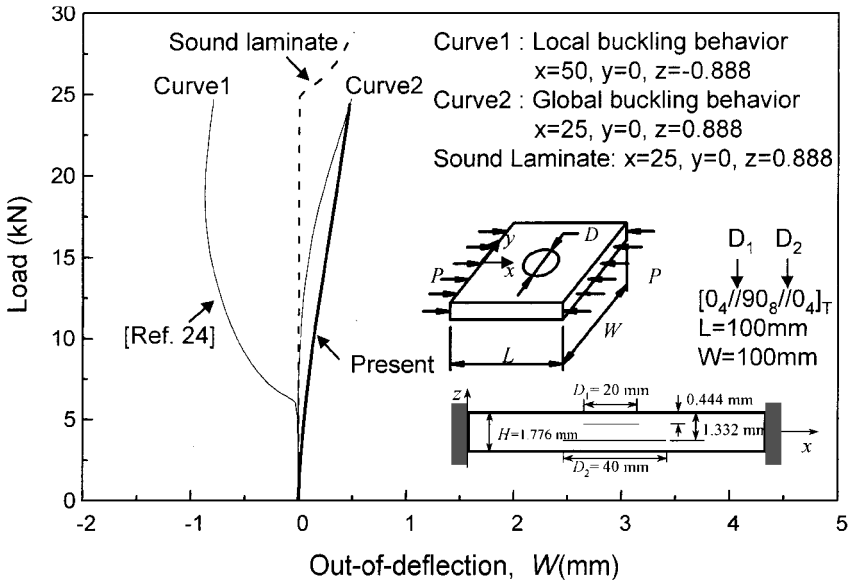


**Fig. 2 Comparison of present analysis with local/global buckling analysis.**

ratio of the $i$th sublaminates. The axial, transverse, and shear moduli of the $i$th sublaminate in the degradation region were multiplied by the same retention ratio:

$$E_1^{i^*} = R_i E_1^i, \qquad E_2^{i^*} = R_i E_2^i, \qquad G_{12}^{i^*} = R_i G_{12}^i \tag{2}$$

The nonlinear finite element equation[22] is expressed as

$$([K_L] + [K_{NL}])\{\Delta U_n\} = -\{\Delta P\} \tag{3}$$

where

$$[K_L] = \iiint_{V^n} \left[B_L^n\right]^T [D^n] \left[B_L^n\right] \mathrm{d}V \tag{4}$$

$$[K_{NL}] = \iiint_{V^n} \left[B_{NL}^n\right]^T [\bar{\sigma}^n] \left[B_{NL}^n\right] \mathrm{d}V \tag{5}$$

$$\{\Delta P\} = \iiint_{V^n} \left[B_L^n\right]^T \{\sigma^n\} \mathrm{d}V - \{F_n\} \tag{6}$$

From the preceding equations, $n$, $[K_L]$, $[K_{NL}]$, $\{\Delta U\}$, $[D]$, $\{\Delta P\}$, and $\{F_n\}$ are the iteration step in any load step, the linear stiffness element matrix, the nonlinear stiffness element matrix, the displacement vector, the stress–strain relation matrix, the unbalanced force, and the external force-distribution vector, respectively. Also, $[B_L]$, $[B_{NL}]$, $\{\sigma\}$, and $\bar{\sigma}$ can be found in Ref. 23. To estimate the failure load, the maximum stress criterion is applied to the average stresses in the principal material directions of each layer of each element. The failure of each element in the model is estimated for the converged stresses during each load step:

$$\begin{aligned} \sigma_1^m > X_T \quad &\text{or} \quad \sigma_1^m < X_C \\ \sigma_2^m > Y_T \quad &\text{or} \quad \sigma_2^m < Y_C \\ \tau_{12}^m > S \quad &\text{or} \quad \tau_{12}^m < -S \end{aligned} \tag{7}$$

From Eqs. (7), $X$, $Y$, and $S$ are the strength in the fiber direction, the strength in the transverse direction, and the shear strength, respectively. $T$, $C$, and $m$ are the tension, the compression, and the mean value, respectively. The stress and the stiffness component corresponding to the particular failure mode were reduced to zero. The maximum stress criterion and the complete unloading model were applied to all areas of the structures including the delaminated region. Generally, the buckling does not indicate final failure, and the postbuckling is indicative of the ability of a structure to carry loads well in excess of the buckling load. The upper limit of the postbuckling range is the compressive strength. Therefore, the final failure was determined at the point where the load decrease began in the postbuckling region due to failure.

In the present analysis, the effects of local impact damages on the global buckling were considered in the finite element model by introducing the stiffness reduction region instead of a local buckling analysis. We analyzed the postbuckling and the failure by using the stiffness reduction model. The postbuckling failure modes were matrix, shear, and fiber failure. A traditional local/global buckling analysis was very complex and inefficient for the postbuckling failure analysis of an unstiffened plate or stiffened plates with impact damage. Therefore, one of the main objectives is to analyze the global buckling and the postbuckling failure using the stiffness reduction model instead of a local buckling analysis.

Figure 2 shows the comparison of the present global buckling analysis using the stiffness reduction model with the traditional local/global buckling analysis.[24] Two delaminations with different diameters exist in composite laminates, and the boundaries are four fixed sides. The analysis prevented the overlapping between the delaminated plies. Curve 1 is the local buckling behavior of delaminated plies, and curve 2 is the global buckling behavior of the sound plate. Sound laminate indicates the global buckling behavior of the sound plate. Though there is a little difference for the global buckling behavior between the present analysis and the local/global

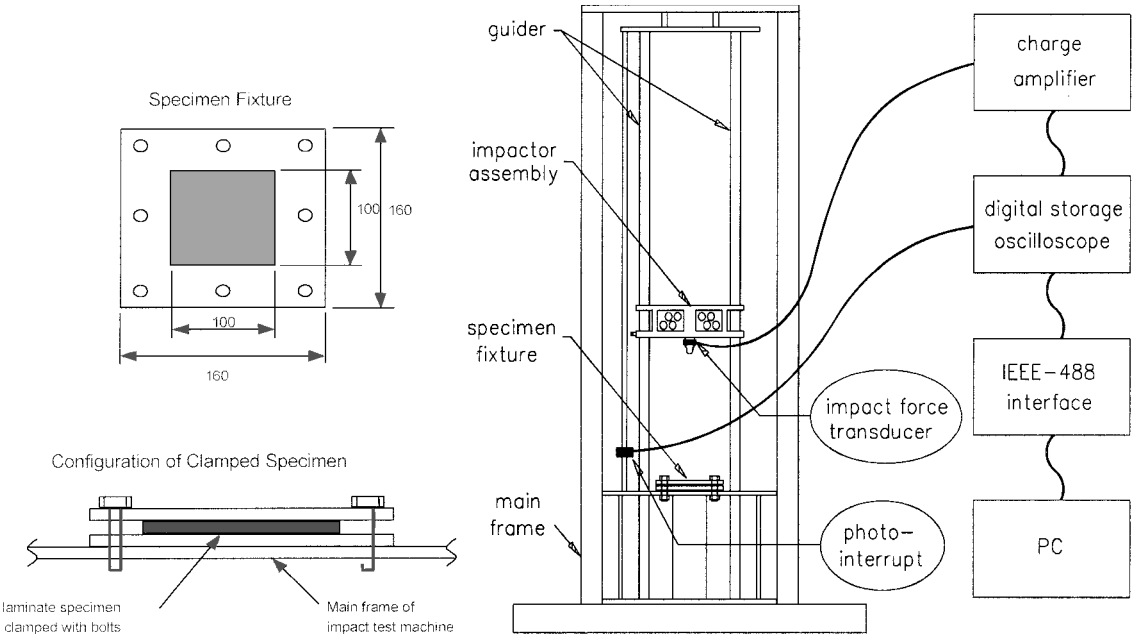


**Fig. 3 Schematic diagram for drop-weight impact system.**

buckling analysis, the present analysis showed the global buckling behavior of the damaged laminate well. The reason for the difference is that the local/global buckling analysis assumed the impact damages to be only delaminations in which the delaminated plies carried a compressive load. However, the present analysis assumed that the impact damaged plies did not carry the compressive load.

## Experiments

A drop-weight impact testing machine[25] was used for the low-speed impact test as shown in Fig. 3. The machine consists of two vertical steel rods mounted on a heavy steel base. A piezoelectric force transducer (208C05 PCB; PCB Piezoelectric, Inc.) with a hemispherical steep cap was mounted on the bottom side of the impactor assembly. The total mass of the whole drop weight was 1.0 kg. The impactor had a hemispherical nose of 12.7 mm in diameter. The boundary conditions of the unstiffened plate were fixed along the four edges.

After impact tests, each specimen was inspected by using C-SCAN (USD-10; Krautkrämer Co.). Figure 4 shows the experimental setup for C-SCAN. This tester has a probe for both the emission and the reception of the ultrasonic wave. This tester has two detecting modes, the amplitude and the depth modes. The amplitude mode detects the damage in the specimen by measuring the ultrasonic echo amplitude. To not measure the echo amplitude reflecting from the bottom surface, the operator must exclude the bottom peak level from the gate. However, the depth mode measures the echo delay. Thus, the damage is represented in terms of the relative depth. Figure 5 shows several echo peaks due to medium discontinuity at interlaminar surfaces. In this study, a gating technique was utilized to detect the delamination distributions through the thickness. For example, if a specimen has two delaminations as shown in Fig. 5a, USD-10 shows two high peaks. In the conventional amplitude mode method, the USD-10 measures only the highest peak level in the fifth interface. In the present method, both the second and the fifth peak levels could be detected by controlling the gate size as shown in Fig. 5b.

To demonstrate this method, the deply technique and the gating technique is shown in Fig. 6a. The stacking sequence was $[0_2/45_2/-45_2/90_2]_s$, and impact energy levels were 5 and 3 J, respectively. In case of 5 J, the delamination shapes obtained by the deply technique[26] were identical to the delamination shapes detected by the gating technique. The delamination shape of the lowest interface captured by the gating technique was not identical to the original form obtained by the deply technique. Because the interference of the high echo amplitude, which was reflected from the

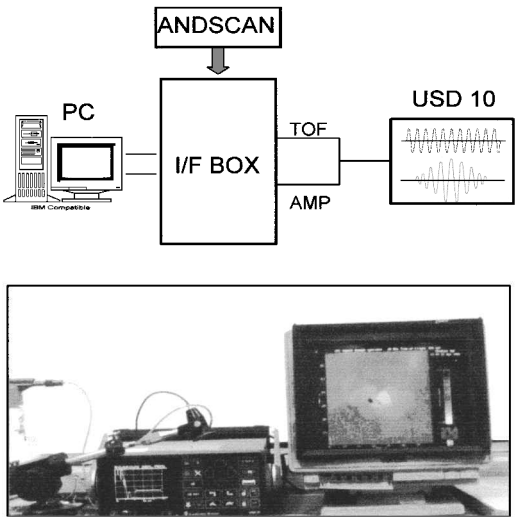


**Fig. 4 Experimental setup for C-SCAN.**

bottom surface, hindered the maximum use of the high echo amplitude gain, we could not eliminate the shadow effect. However, if the inspection was made from the opposite side, or the peak of the bottom was separated far from that of the last interface, the original shape could be precisely detected.

## Compression Test

After the ultrasonic detection of the impact damage, the specimens were tested under compression. In the case of the stiffened composite plates, the loaded ends were potted in the casting resin, and they were machined flat and normal to the loading direction uniformly. The loading rate was 0.5 mm/min. The panels were painted white and the out-of-plane deflections were also monitored by the shadow moiré technique.

## Results and Discussion

### Unstiffened Composite Plates

The graphite/epoxy was CU-125NS and was made by the Korea Carbon Company. The ply thickness was 0.125 mm. The material properties were $E_1 = 130.0$ GPa, $E_2 = E_3 = 10.0$ GPa, $G_{12} = G_{13} = 4.85$ GPa, $G_{23} = 3.62$ GPa, $\nu_{12} = \nu_{13} = 0.31$, $\nu_{23} = 0.52$, $X_T = 1933$ MPa, $X_C = 1051$ MPa, $Y_T = 51$ MPa, $Y_C =$

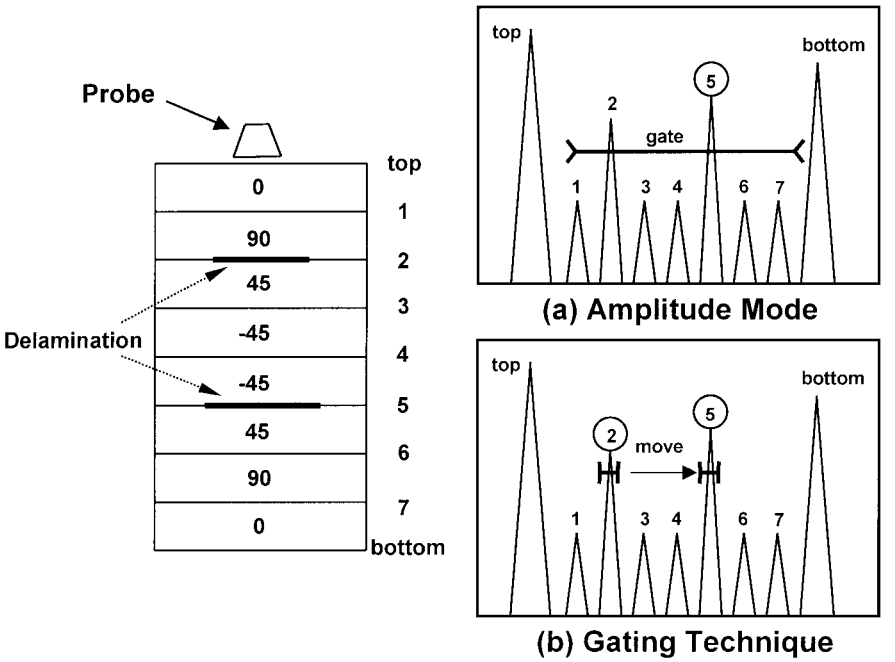


**Fig. 5 Gating technique for detection of ply-by-ply delaminations.**

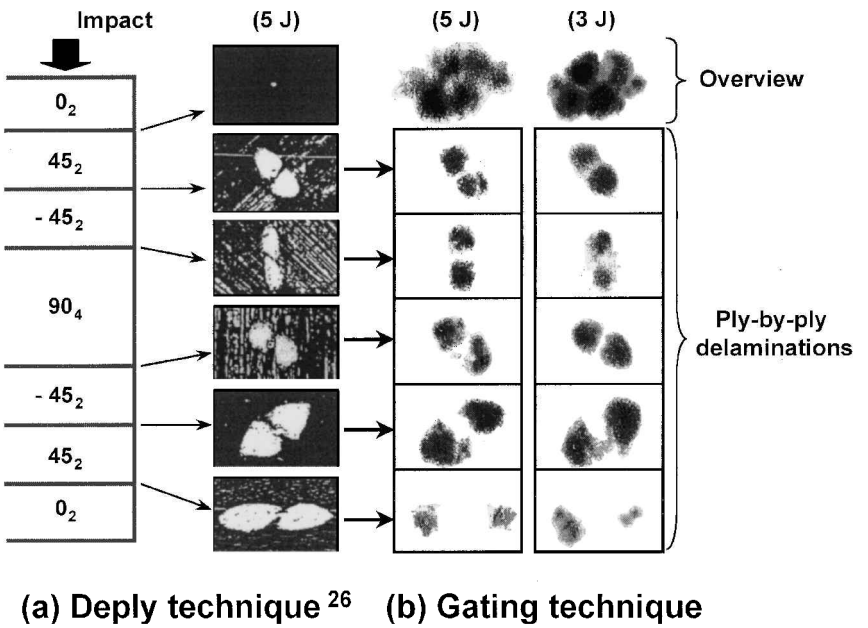


**Fig. 6 Comparison of the gating technique with deply technique.**

141 MPa, and $S = 61$ MPa, where $X$ is the strength in the fiber direction, $Y$ is the strength in transverse direction, and subscripts $T$ and $C$ represent tension and compression, respectively. The $[0_4/45_4/90_4/45_4/0_4]_T$ laminates were used to demonstrate the prediction method of the residual strength. For the impact test of the plates, the composite plates were clamped along the four edges by supporting the fixture.

Typical delamination distributions through the thickness are shown in Fig. 7. In the case of 9 J, the delamination shape in the bottom was irregular because the backface crack occurred. The delamination sizes with various impact energy levels are summarized in Table 1 and Fig. 8. The selected energy levels were 1, 2, 3, 4.5, 6, and 9 J. The difference between the summation of ply-by-ply delamination areas and the two-dimensional projected delamination area became larger as the impact energy level increased. Therefore, the two-dimensional projected delamination area could not represent the real impact damage when the impact energy was large. The

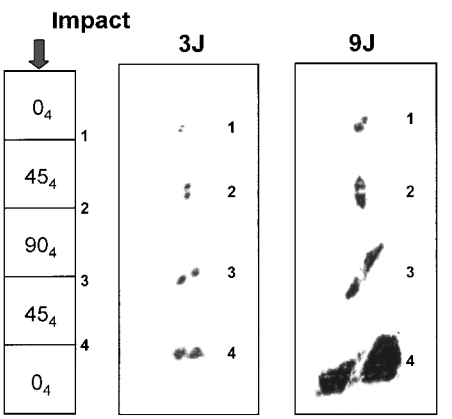


**Fig. 7 Delamination shapes of typical plates.**

**Table 1 Delamination area of the composite plates ($[0_4/45_4/90_4/45_4/0_4]_T$)**

| Impact energy, J | Delamination area through the thickness direction, mm$^2$ | | | | | |
|---|---|---|---|---|---|---|
| | $0_4//45_4^a$ | $45_4//90_4$ | $90_4//45_4$ | $45_4//0_4$ | Three-dimensional summation | Two-dimensional projection |
| 1 | 0 | 21 | 36 | 53 | 110 | 73 |
| 2 | 35 | 96 | 93 | 165 | 389 | 342 |
| 3 | 38 | 124 | 116 | 239 | 517 | 439 |
| 4.5 | 65 | 127 | 186 | 530 | 908 | 764 |
| 6 | 67 | 192 | 372 | 1884 | 2516 | 2038 |
| 9 | 124 | 287 | 571 | 2794 | 3776 | 2985 |

[a]The double slash (//) means the interface where delamination was inspected by C-SCAN.

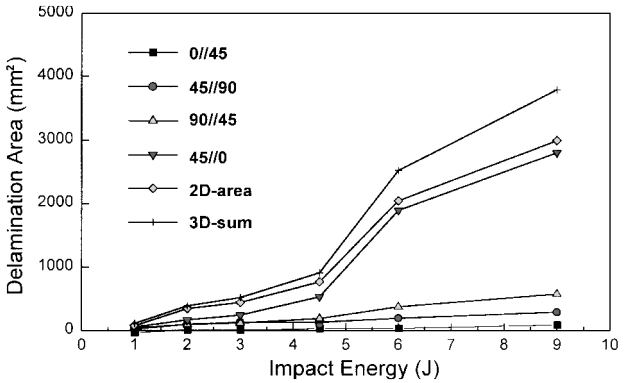


**Fig. 8 Delamination sizes with various impact energy levels.**

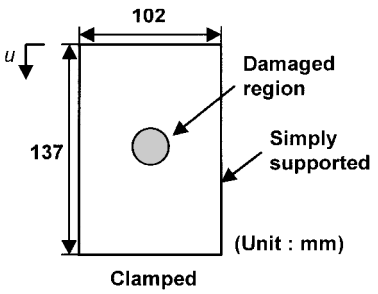


**Fig. 9 Geometry and boundary conditions of unstiffened plates.**

modulus retention ratio of the impact-damaged region was determined by Eq. (1). The stiffness reduction region in the analysis was modeled as a circular hole as shown in Fig. 9. The boundaries are clamped at the loaded edges and simply supported along the unloaded sides. We analyzed the buckling and the postbuckling failure using this stiffness reduction model.

The results of the compressive strength study are shown in Fig. 10, where $\sigma_0$ is the experimental strength of the undamaged plate and $\sigma_r$ is the residual strength of the damaged plate. The postbuckling compressive strength of the undamaged panel was 39.4 kN in the experiment and 49.2 kN in the analysis. The present analysis relative to the tendency of the postbuckling compressive strength showed good agreement with the experimental results. The decrease of the residual strength was proportional to the summation of ply-by-ply delamination after 4.5 J. When the damaged region was assumed as a cutout in the case of 6 J, the residual strength was 36% lower than that of the present model.

To observe the delamination growth in the present specimen, we inspected the specimen by C-SCAN near final failure. The load level was 90% of the compressive strength of the specimen. As shown in Fig. 11, dominant delamination growth was not found in each interface. Therefore, the cause of the compressive strength reduction was not the delamination growth, but the stiffness reduction in the damaged region. Figure 12a shows the specimen after the final failure. Final failure modes had several failure modes such as the fiber failure, the surface cracking, and the delamination failure. Final failure modes occurred just before the collapse of the specimen. Figure 12b shows the result of the progressive failure analysis in the case of 6 J. The first failure occurred in the stiffness reduction area, region A, at 72% of the compressive strength. The failure in undamaged area, region B, occurred at 91% of the compressive strength. Though the delamination fail was not predicted in the progressive failure analysis, the failure mechanism was similar to that in the experiment.

**Stiffened Composite Plates**

The shape and the dimension of the blade-stiffened plate are shown in Fig. 13. The impact location was over the edge of the flange. The buckling load was detected by back-to-back strain gauges in the skin. The stiffener and the skin were bonded with FM73 adhesive film. After curing, the stiffened panels were inspected by C-SCAN, and no significant defects were detected. The stiffener and the skin have the same layup sequence of $[0_2/45_2/-45_2/90_2]_s$.

Two stiffened plates were tested per one impact energy level. The impact energy levels were 0, 5, and 9 J. The delamination distributions of the blade-stiffened plate with 5-J damage are shown in Fig. 14. The delamination shapes in the upper skin were similar to those of the unstiffened plate. However, the shapes were a little different in the bottom skin due to the stiffener. The delamination shapes of the flange part were inspected from the backside. The gate interval was enlarged because the delamination distributions in the flange had no clear shape. The two-dimensional projected delamination shape was a rectangle, and the major axis was parallel to the stiffener.

The comparison of the impact damages between the stiffened plate and the unstiffened plate, which have the same boundary conditions and stacking sequences, is shown in Fig. 15. The delamination area of the unstiffened plate was smaller than the area of the stiffened plate. The unstiffened plate had fiber failure and cracks in the backside. However, the stiffener of the stiffened plate suppressed both the fiber failure and the backface crack, and impact energy was mainly absorbed by delaminations.

The delamination sizes, according to the various impact energy levels, are summarized in Table 2 and Fig. 16. The two-dimensional projected area of 9 J was twice as large as that of 5 J, and the three-dimensional summation area of 9 J was also twice as large as that of 5 J. Therefore, the increase rate of the two-dimensional projected area was proportional to that of the three-dimensional summation area. The modulus retention ratios of the impact-damaged region were determined by Eq. (1). The damaged region in the analysis was assumed to be a rectangle.

The buckling and postbuckling residual strengths are shown in Figs. 17 and 18. The averaged buckling load of an undamaged panel was 27.5 kN in the experiment and 24.6 kN in the analysis. The averaged postbuckling compressive strength of the undamaged panel was 48.5 kN in the experiment and 60.6 kN in the analysis. The reductions of buckling load were 10% (analysis) and 9% (experiment) in the case of 5 J. Also, the reductions of buckling load were 18% (analysis) and 24% (experiment) in the case of 9 J. The reductions of the postbuckling compressive strength were dominant for 9 J, both for the analysis and for the experiment. The present analyses relative to the tendency of the buckling and postbuckling compressive strength showed good agreement with the experimental results.

In the case of a $[0_2/45_2/-45_2/90_2]_s$ unstiffened plate damaged by a 5-J impact, the reduction ratio of the compressive strength was 65% in the earlier experiment,[26] but that of the blade-stiffened plate was almost equal to the undamaged case. Therefore, the stiffener increased the damage tolerance of the composite plate. The

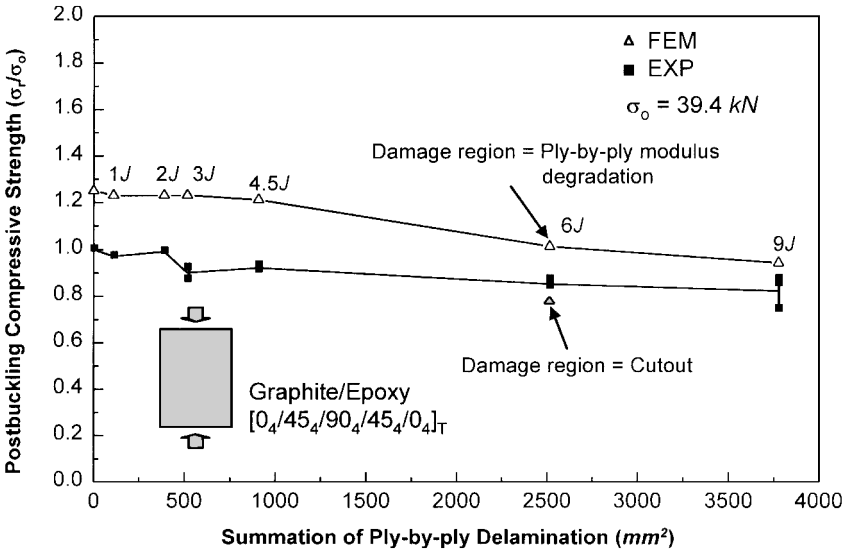


**Fig. 10 Postbuckling compressive strength of unstiffened plates with various impact energies.**

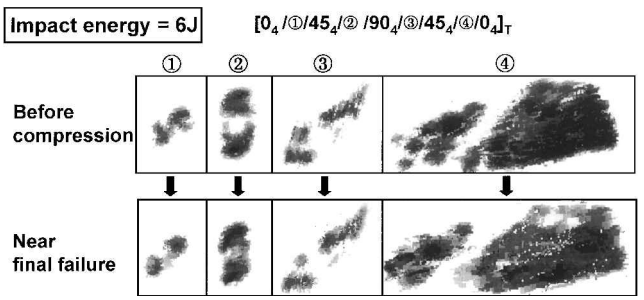


**Fig. 11 Observation of delamination shapes during compression.**

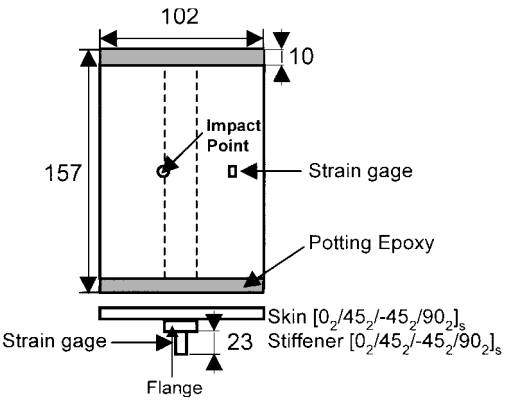


**Fig. 13 Geometry and boundary conditions of blade-stiffened composite plates.**

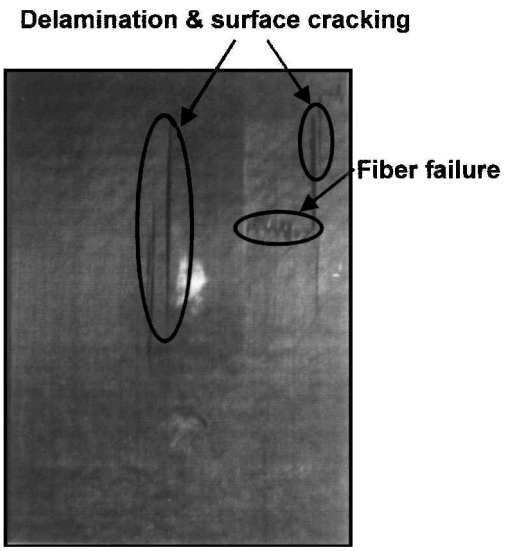


a)

Progressive failure analysis (6J)

A=stiffness reduction region
B=sound region

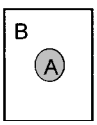


| | Failure (region A) | Failure (region B) | Final failure |
|---|---|---|---|
| Failure / Final failure | 0.72 | 0.91 | 1 |

b)

**Fig. 12 Failure modes of specimen and failure region in analysis.**

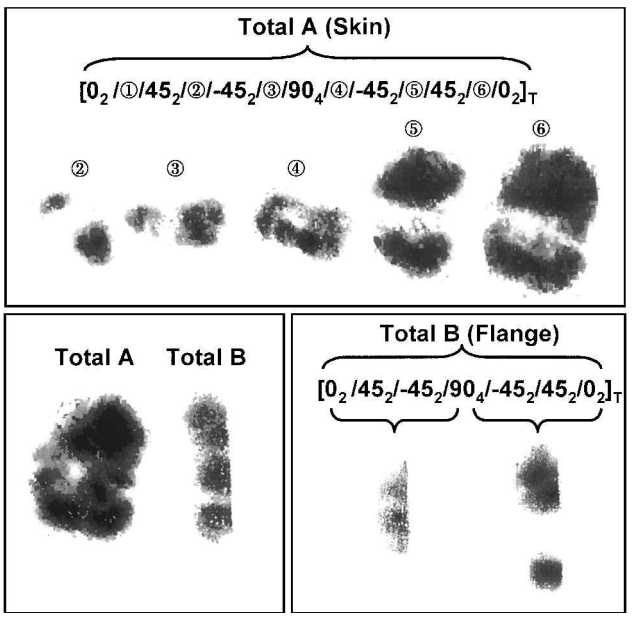


**Fig. 14 Delamination shapes of stiffened plate damaged by 5 J impact.**

postbuckling mode in the 5- and 9-J cases are shown in Fig. 19. The moiré fringe showed the local buckling due to the large delamination of the skin in case of 9 J, but no local buckling was observed in case of 5 J up to the final failure. Therefore, the stiffness reduction of 9 J was larger than that of 5 J. In Fig. 19, the load level of 9 J-A was 66% of the final failure and that of 9 J-B was 99%. No dominant delamination growth was observed in either case. Therefore, the reduction of the compressive strength was mainly due to the reduction of the stiffness in the damaged region similar to the unstiffened plates.

**Damage Growth Under Cyclic Compression**

The shape and dimensions of I-stiffened plates are shown in Fig. 20. The stiffened panels consist of two stiffeners that have the layup sequences of $[0/90/45/0/-45]_S$ (Ref. 27). The stiffened panels were 160 mm wide × 250 mm long, and the stiffeners were 100 mm apart. The impact point was the skin bay or the skin over the stiffener. Two stiffened plates were tested for each impact location, and the impact energy was 1.5 J. The static compression test results for first-fiber (FFF), first-matrix (FMF), and first-shear failures (FSF) are shown in the progressive analysis in Fig. 21.

To observe damage growth according to the impact locations, we have performed the fatigue tests of impact-damaged stiffened plates. The cyclic compressive load was applied between 15 and 30% of the static strength as shown in Fig. 21. The buckling occurred repeatedly in this range. The cyclic frequency was 4.3 Hz and 120,000 cycles were applied. Table 3 shows delamination areas, and Fig. 22 shows delamination shapes. The overall delamination shape was circular in the case of impact on the skin bay. The major axis of the delamination shape in the case of the impact over the stiffener was parallel to the stiffener. The dominant delamination growth, which crossed the web line, was observed in the case of impact over the stiffener. The time-strain curve of this case is shown in Fig. 23. Strain gauges were bonded at the impact point. The strain suddenly increased at the lapse of 20,000 cycles, and the increased strain did not change

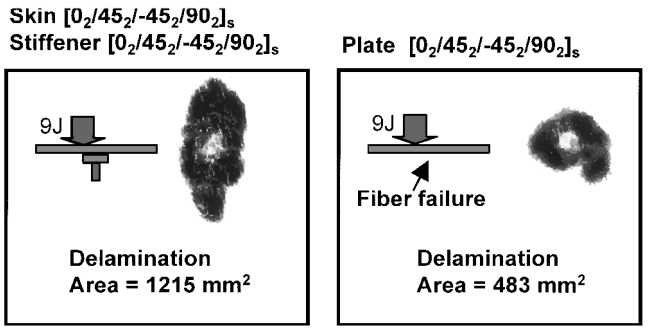


**Fig. 15 Comparison of stiffened plate with unstiffened plate about impact damage.**

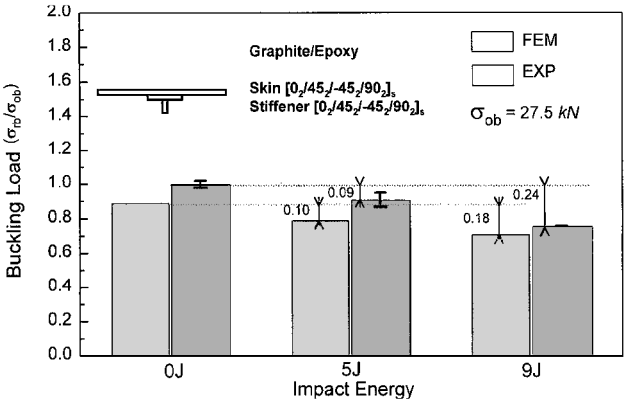


**Fig. 17 Buckling load of stiffened plates with various impact energies.**

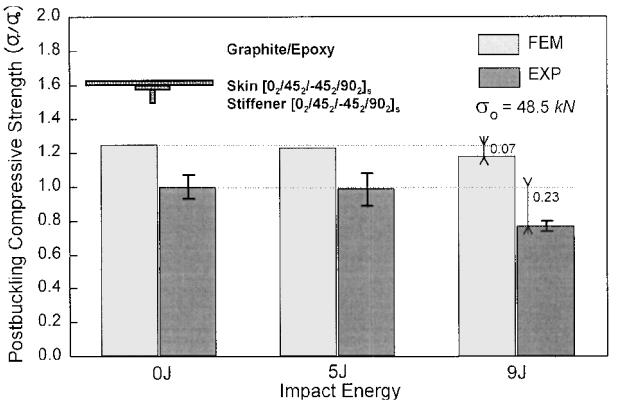


**Fig. 18 Postbuckling compressive strength of stiffened plates with various impact energies.**

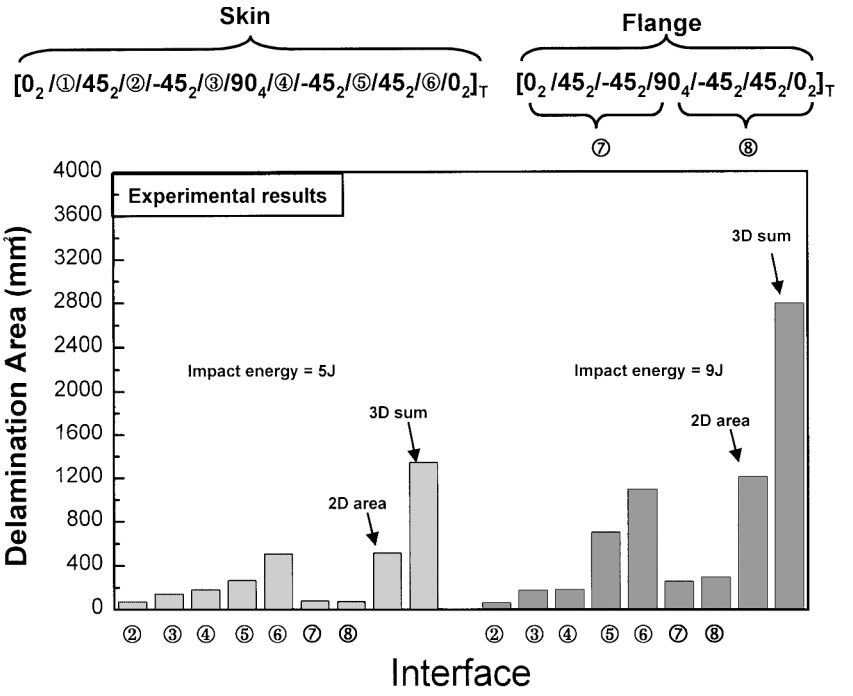


**Fig. 16 Delamination sizes through the thickness.**

**Table 2 Delamination area of the blade stiffened plates[a]**

| Impact energy, J | Delamination area of the skin part, mm$^2$ | | | | | | Delamination area of the flange part, mm$^2$ | | |
|---|---|---|---|---|---|---|---|---|---|
| | $45_2//-45_2^b$ | $-45_2//90_2$ | $90_2//-45_2$ | $-45_2//45_2$ | $45_2//0_2$ | Two-dimensional projection | $0_2//45_2//-45_2//90_2$ | $90_2//-45_2//45_2//0_2$ | Two-dimensional projection |
| 5 | 76 | 146 | 186 | 269 | 511 | 520 | 83 | 78 | 100 |
| 9 | 64 | 180 | 186 | 710 | 1100 | 1215 | 260 | 300 | 327 |

[a]Skin: $[0_2/45_2/-45_2/90_2]_s$, stiffener: $[0_2/45_2/-45_2/90_2]_s$. [b]The double slash (//) means the interface where delamination was inspected by C-SCAN.

**Table 3 Delamination area of the I-stiffened plates[a]**

| Impact location | Two-dimensional delamination area, mm$^2$ | | |
|---|---|---|---|
| | Before fatigue | After fatigue | Difference |
| Midbay | 58 (58)[b] | 71 | 13 |
| Stiffener | 186 (174) | 313 | 127 |

[a]Skin: $[0/90/\pm45]_s$, stiffener: $[0/90/45/0/-45]_s$.
[b]( ) Contain the other specimens results, to compare impact damages.

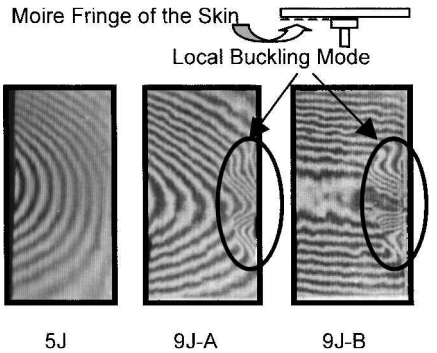


**Fig. 19 Buckling mode of stiffened plates obtained by moiré fringe.**

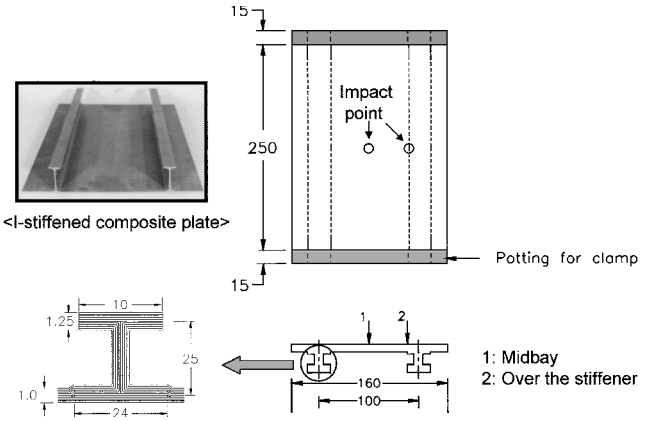


**Fig. 20 Impact locations of I-stiffened composite plates.**

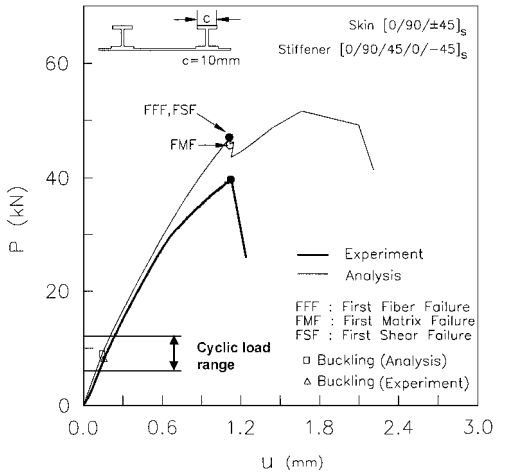


**Fig. 21 Cyclic load range of I-stiffened composite plates.**

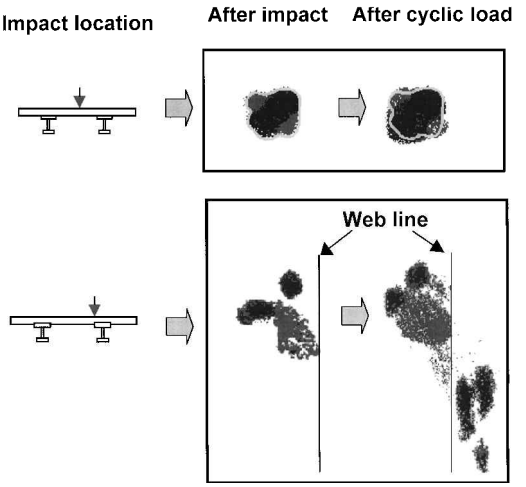


**Fig. 22 Delamination growth according to impact locations.**

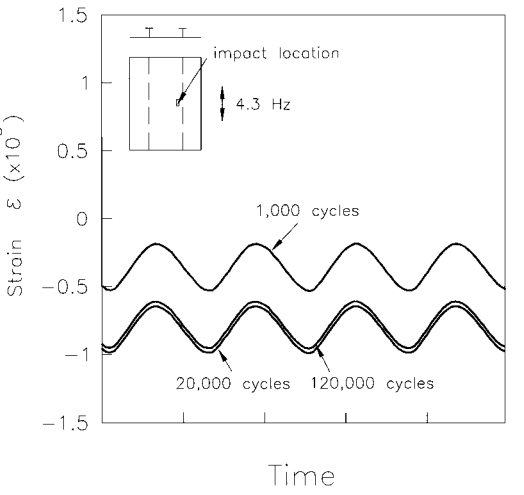


**Fig. 23 Time-strain curve during cyclic compression.**

until 120,000 cycles. These results showed that the delamination growth started at about 20,000 cycles.

## Conclusions

The effects of impact damage on buckling and postbuckling strength were studied numerically and experimentally. In the numerical analysis, a progressive failure model with degradation of elastic moduli in the damaged region was adopted in the global postbuckling analysis instead of a local/global buckling analysis. The modulus retention ratios were determined by delamination distributions obtained from the improved ultrasonic inspection that has two-ply resolutions. The difference between the summation of ply-by-ply delamination and the two-dimensional projected area increased as impact energy became greater. The increase rate of the two-dimensional area was proportional to that of the three-dimensional summation area. In the CAI tests, the limited delamination growth, which did not lead to the final failure, was observed by C-SCAN and the moiré technique. The present analysis relating the tendency of the buckling and postbuckling strength with incremental

impact energy showed good agreement with experimental results. The summation of ply-by-ply delamination was closely related to the residual strength of composite structures. The impact damage of the stiffened composite plates was mainly delamination because the stiffener suppressed the fiber failure and the backface cracks. The stiffener increased the damage tolerance of the unstiffened composite plates. Delamination growth of the I-stiffened composite plates under the cyclic compressive load was also observed according to the impact locations. The dominant damage growth was observed in the case of an impact over the stiffener.

## Acknowledgment

The authors are grateful for the financial support of the Korea Agency for Defense Development (Project ADD-98-5-002).

## References

[1]Shyprykevich, P., "Damage Tolerance of Composite Aircraft Structures: Analysis and Certification," *Proceedings of the Eleventh International Conference on Composite Materials (ICCM-11)*, edited by M. L. Scott, Woodhead Publishing, Ltd., Gold Coast, Australia, 1997, pp. 1.519–1.526.

[2]Ishikawa, T., Sugimoto, S., Matsushima, M., and Hayashi, Y., "Some Experimental Findings in Compression-After-Impact (CAI) Tests of CF/peek (APC-2) and Conventional CF/epoxy Flat Plates," *Composite Science and Technology*, Vol. 55, 1995, pp. 349–363.

[3]Chen, V. L., Wu, H. Y., and Yeh, H. Y., "A Parametric Study of Residual Strength and Stiffness for Impact Damaged Composites," *Composite Structures*, Vol. 25, 1993, pp. 267–275.

[4]Zhou, G., "The Use of Experimentally-Determined Impact Force as a Damage Measure in Impact Damage Resistance and Tolerance of Composite Structures," *Composite Structures*, Vol. 42, 1998, pp. 375–382.

[5]Palazotto, A. N., Gummadi, L. N. B., Vaidya, U. K., and Herup, E. J., "Low Velocity Impact Damage Characteristics of Z-fiber Reinforced Sandwich Panels—An Experimental Study," *Composite Structures*, Vol. 43, 1999, pp. 275–288.

[6]Pavier, M. J., and Clarke, M. P., "Finite Element Prediction of the Post-Impact Compressive Strength of Fibre Composites," *Composite Structures*, Vol. 36, 1996, pp. 141–153.

[7]Xiong, Y., Poon, C., Straznicky, P. V., and Vietinghoff, H., "A Prediction Method for the Compressive Strength of Impact Damaged Composite Laminates," *Composite Structures*, Vol. 30, 1995, pp. 357–367.

[8]De Moura, M. F. S. F., Goncalves, J. P. M., Marques, A. T., and De Castro, P. M. S. T., "Modeling Compression Failure after Low Velocity Impact on Laminated Composites Using Interface Elements," *Journal of Composite Materials*, Vol. 31, No. 15, 1997, pp. 1462–1479.

[9]Gottesman, T., Girshovich, S., Drukker, E., Sela, N., and Loy, J., "Residual Strength of Impacted Composites: Analysis and Tests," *Journal of Composite Technology and Research*, Vol. 16, No. 3, 1994, pp. 244–255.

[10]Scarponi, C., Briotti, G., Baroboni, R., Marcone, A., and Iannone, M., "Impact Testing on Composite Laminates and Sandwich Panels," *Journal of Composite Materials*, Vol. 30, No. 17, 1996, pp. 1873–1911.

[11]Madan, R. C., and Shuart, M. J., "Impact Damage and Residual Strength Analysis of Composite Panels with Bonded Stiffeners," *Composite Materials: Testing and Design*, Vol. 9, edited by S. P. Garbo, ASTM Special Technical Publication (STP) 1059, American Society for Testing and Materials, Philadelphia, 1990, pp. 64–85.

[12]Greenhalgh, E., Bishop, S. M., Bray, D., Hughes, D., Lahiff, S., and Millson, B., "Characterization of Impact Damage in Skin-Stringer Composite Structures," *Composite Structures*, Vol. 36, 1996, pp. 187–207.

[13]Greenhalgh, E., Singh, S., and Roberts, D., "Impact Damage Growth and Failure of Carbon-Fibre Reinforced Plastic Skin-Stringer Panels," *Proceedings of the Eleventh International Conference on Composite Materials (ICCM-11)*, edited by M. L. Scott, Woodhead Publishing, Ltd., Gold Coast, Australia, 1997, pp. 2.573–2.582.

[14]Ishikawa, T., Matsushima, M., and Hayashi, Y., "Improved Correlation of Predicted and Experimental Initial Buckling Stress of Composite Stiffened Panels," *Composite Structures*, Vol. 36, 1993, pp. 25–38.

[15]Found, M. S., Howard, I. C., and Paran, A. P., "Impact Behavior of Stiffened CFRP Sections," *Composite Structures*, Vol. 39, 1997, pp. 229–235.

[16]Starnes, J. H., Jr., Knight, N. F., Jr., and Rouse, M., "Postbuckling Behavior of Selected Flat Stiffened Graphite-Epoxy Panels Loaded in Compression," *AIAA Journal*, Vol. 23, No. 8, 1985, pp. 1236–1246.

[17]Kim, H. J., and Hong, C. S., "Buckling and Postbuckling Behavior of Composite Laminates with a Delamination," *Composite Science and Technology*, Vol. 57, 1997, pp. 557–564.

[18]Kyoung, W. M., Kim, C. G., Hong, C. S., and Jun, S. M., "Modeling of Composite Laminates with Multiple Delaminations Under Compressive Loading," *Journal of Composite Materials*, Vol. 32, No. 10, 1998, pp. 951–968.

[19]Suemasu, H., Kumagai, T., and Gozu, K., "Compressive Behavior of Multiply Delaminated Composite Laminates Part1: Experiment and Analytical Development," *AIAA Journal*, Vol. 36, No. 7, 1998, pp. 1279–1285.

[20]Gu, H., and Chattopadhyay, A., "Delamination Buckling and Postbuckling of Composite Cylindrical Shells," *AIAA Journal*, Vol. 34, No. 6, 1996, pp. 1279–1286.

[21]Comiez, J. M., Waas, A. M., and Shahwan, K. W., "Delamination Buckling; Experiment and Analysis," *International Journal of Solids and Structures*., Vol. 32, No. 6/7, 1995, pp. 767–782.

[22]Kweon, J. H., Hong, C. S., and Lee, I. C., "Postbuckling Compressive Strength of Graphite/Epoxy Laminated Cylindrical Plates Loaded in Compression," *AIAA Journal*, Vol. 33, No. 2, 1995, pp. 217–222.

[23]Bathe, K. J., *Finite Element Procedures in Engineering Analysis*, Prentice–Hall, Englewood Cliffs, NJ, 1982.

[24]Kyoung, W. M., Kim, C. G., and Hong, C. S, "Buckling and Postbuckling Behavior of Composite Cross-Ply Laminates with Multiple Delaminations," *Composite Structures*, Vol. 43, 1999, pp. 257–274.

[25]Choi, I. H., and Hong, C. S., "Low-Velocity Impact Response of Composite Laminates Considering Higher-Order Shear Deformation and Large Deflection," *Mechanics of Composite Materials and Structures*, Vol. 1, 1994, pp. 157–170.

[26]Choi, I. H., Choi, Y. R., and Hong, C. S., "Experimental Analysis on Residual Compressive Strength of Graphite/Epoxy and Graphite/Peek Composite Laminates after Low-Velocity Impact," *Journal of the Korean Society for Composite Materials*, Vol. 6, No. 2, 1993, pp. 69–79 (in Korean).

[27]Kong, C. W., Lee, I. C., Kim, C. G., and Hong, C. S., "Postbuckling and Failure of Stiffened Composite Panels Under Axial Compression," *Composite Structures*, Vol. 42, 1998, pp. 13–21.

A. N. Palazotto
*Associate Editor*